

## CFD investigation of fuel property effect on cavitating flow in generic nozzle geometries

Junmei Shi\* and Mohammad Shamsul Arafin  
Continental Automotive GmbH  
Siemensstrasse 12, 93055 Regensburg

### Abstract

This paper reports a numerical study of the effect of fuel property and fuel temperature change on mechanical cavitating flow in generic nozzle geometries. The work was based on the commercial CFD code ANSYS CFX11.0. The liquid and the vapor phase were treated as a homogeneous mixture with a transport equation for the volume fraction of the vapor phase. The cavitation induced inter-phase mass transfer was calculated by a Rayleigh-Plesset-Equation based cavitation model. First, model parameter calibration was carried out and the results were validated against experimental results. Then, investigations were carried out for the effects of three important properties, namely the fuel vapour saturation pressure, density and viscosity, on cavitation behaviour. Simulations were carried out by varying each of the parameters and keeping the other constant in the same time and by varying the temperature for the fuel n-heptane. Their influences on the discharge coefficient, critical cavitation point, vapour volume fraction distribution, and flow velocity development in the nozzle throttle were evaluated. The results indicate a strong influence of Reynolds number on mechanical cavitation phenomenon. In addition, the results were found to be useful for understanding and interpretation of practical spray visualization and engine experiment results.

---

### Introduction

The thermodynamic properties of Diesel or gasoline fuels in the market can vary a lot, because the compositions of the fuels can be very different from oil company to oil company, and even from refinery to refinery, and from production time to production time. Recently, the automotive industry is seeing a big trend in application of regenerative fuels or blending of mineral fuels with high percentage of renewable fuels. Some material parameters of these new fuels such as density, viscosity and vapour saturation pressure differ very much from the traditional mineral fuels. In addition, fuel properties are affected by operating temperature and pressure. As an example, the fuel viscosity in cold start phase can be doubled compared to the normal operating conditions. Therefore, two points are of practical importance for the direct injection technology development and validation. One is the fuel property under real engine operating conditions. The other is about the effect of fuel properties on the hydraulic flow, atomization of an injection nozzle and mixture formation in engine. The research in this direction is still very limited, except for some recent work [1-4]. The present numerical study is to investigate the fuel density, viscosity and vapour saturation pressure on the cavitating flow behaviour in fuel injection nozzle by using generic rectangular throttle geometries. First, numerical simulation was carried out for a model Diesel fuel. The results were compared to experimental data established at Continental Automotive GmbH for model validation purpose. Then the investigation was realized by varying one of the parameters and keeping the other unchanged in order to get a clear conclusion about the effect of each parameter. With the background of gasoline direct injection technology development, simulation was also carried out for n-heptane at various temperatures. Their effects on the discharge coefficient, critical cavitation point, vapour volume fraction distribution, and the velocity profile development along the throttle were evaluated.

### Numerical Model

The work was based on the commercial CFD code ANSYS CFX11.0. The liquid and the vapour phase were treated as a homogeneous mixture with a transport equation for the volume fraction of the vapour phase. The CFX  $k-\omega$  SST model [5] was applied for turbulence modelling. A constant pressure 100 bar was assigned at inlet in all cases, while the outlet pressure was varied from 80 to 10 bar. Two nozzle geometries were considered in this work, *geometry J* has a rounding inlet radius 25 $\mu$ m (Fig. 1) while *geometry I* has no inlet rounding. The throttle part has 1 mm in length ( $x$ -direction), 0.299 mm in height ( $y$ -direction) and width ( $z$ -direction). In front of the throttle the channel height is 3 mm, while the width is the same as in the throttle. By assuming stationary and symmetrical flow, simulation was performed based on  $\frac{1}{4}$ -th of the rectangular throttle geometry. This is a good compromise between quality and computational effort, because this simplification was found to have little effect on cavitation in the throttle. The governing equations are as follows

---

\* Corresponding author: Junmei.Shi@continental-corporation.com

$$\frac{\partial \rho_v \alpha_v U_i}{\partial x_i} = S_{lv}$$

$$\frac{\partial \rho_m U_i U_j}{\partial x_i} = -\frac{\partial p}{\partial x_i} + \frac{\partial \tau_{ij}}{\partial x_j}, \text{ with } \tau_{ij} = (\mu_m + \mu_{mt}) \left( \frac{\partial U_i}{\partial x_j} + \frac{\partial U_j}{\partial x_i} \right)$$

where  $U_i, U_j$  are the Reynolds averaged velocity component,  $\alpha$  is the vapour volume fraction,  $\rho_m = \alpha \rho_v + (1 - \alpha) \rho_l$  is the mixture density,  $\mu_m$  the mixture dynamic viscosity, and  $\mu_{mt} = f(\rho) \frac{k}{\omega}$  the viscosity from turbulence modelling.  $S_{lv}$  is the cavitation induced mass source/sink term of the vapour volume fraction transport equation, which was calculated by a Rayleigh-Plesset-Equation (RPE) based cavitation model [6],

$$S_{lv} = \begin{cases} F_1 \frac{3\alpha_0(1-\alpha)\rho_v}{R_b} \sqrt{\frac{2}{3} \frac{p_b - p}{\rho_l}} & \text{if } p < p_b \\ F_2 \frac{3\alpha\rho_v}{R_b} \sqrt{\frac{2}{3} \frac{p - p_b}{\rho_l}} & \text{if } p > p_b \end{cases}$$

Here  $p_b$  is the vapour saturation pressure,  $\alpha_0$  the initial cavitation nuclei volume fraction,  $R_b$  the nuclei bubble radius, and  $F_1, F_2$  the vaporization and condensation coefficient, respectively, to be calibrated. The surface tension effect was neglected in this study.

A second-order discretization was applied for the numerical solution. In order to ensure the quality of the numerical results, grid dependence study was carried out. Finally, the numerical analysis was based on a mesh with c.a. 0.88M cells in size and with local grid refinement in the throttle area.

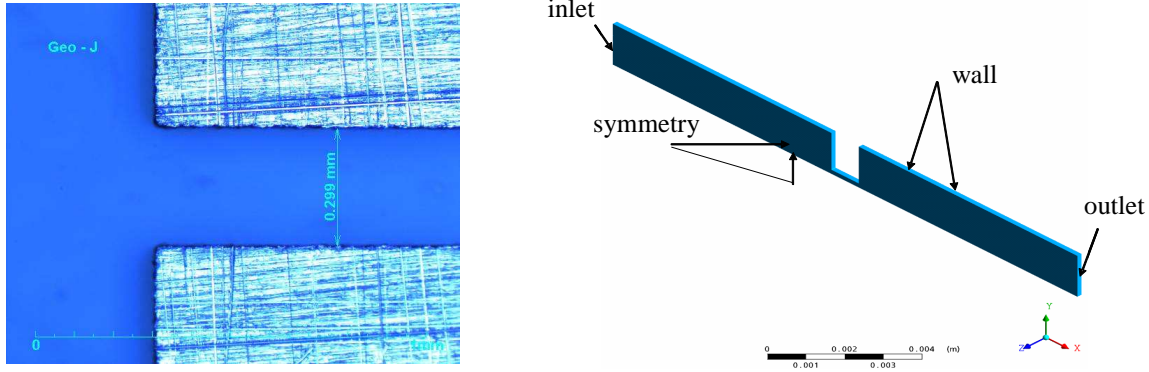


**Figure 1.** Nozzle Jthrottle entrance (left) and the computational domain (right)

## Result and Discussion

### The base case & Model validation

The first step of the study is to do model validation against experimental data based on a model Diesel fuel with a density  $\rho_l = 828 \text{ kg/m}^3$ , a viscosity  $\mu_l = 0.00325 \text{ Pa s}$ , and a vapour saturation pressure  $p_b = 3500 \text{ Pa}$ . Figure 2 shows a comparison of mass flow rate between experimental result and numerical simulation for the geometry J. Satisfactory agreements can be observed. The main deviation is in the critical cavitation point, above which the mass flow become choked, which is about  $\Delta p = 75 \text{ bar}$  in simulation compared with about  $\Delta p = 66 \text{ bar}$  in measurement. However, this deviation can be considered as a systematic error, and thus is not critical for the further investigation of fuel property effects. For the case  $\Delta p = 65 \text{ bar}$ , a comparison of the pressure along the throttle centre line between simulation and measurement is also plotted in Fig. 2 (right). Again, the overall agreement is acceptable in the throttle being aware of the limitation in measurement accuracy. The deviations behind the throttle exit might be due to the application of the  $\frac{1}{4}$  geometrical model and the symmetry boundary conditions in the numerical study. Also, this deviation will not destroy the quality of the current study.

The Reynolds  $Re = \frac{\rho_l V_t L_t}{\mu_l}$  and Cavitation number  $CN = \frac{p_{in} - p_{out}}{p_{out} - p_b}$  corresponding to various pressure differences together the mass flow rate averaged throttle exit velocity of the liquid phase ( $V_{out}$ ) and the volume averaged vapour volume fraction over the computational domain are plotted in Fig. 3. Here  $V_t = \frac{\dot{m}}{\rho_l A_t}$  is the area average liquid velocity at the throttle exit, obtained by dividing the mass flow rate  $\dot{m}$  by the throttle cross-section area  $A_t$  and by the liquid density.  $L_t = 0.299 \text{ mm}$  is the throttle height. It can be observed that cavitation incep-

tion occurs at  $\Delta p > 57$  bar, corresponding to  $Re > 7300$  and to  $CN > 1.33$  in simulation. It is interesting to notice that at  $\Delta p > 70$  bar, the mass flow rate and Reynolds number become constant, but the liquid ejection velocity from the throttle  $V_{out}$ , which is defined as the mass flow rate weighted average liquid velocity at the throttle exit, still increases linearly with increasing  $\Delta p$ . This is due to the reduction of the effective cross-section area caused by increasing cavitation.

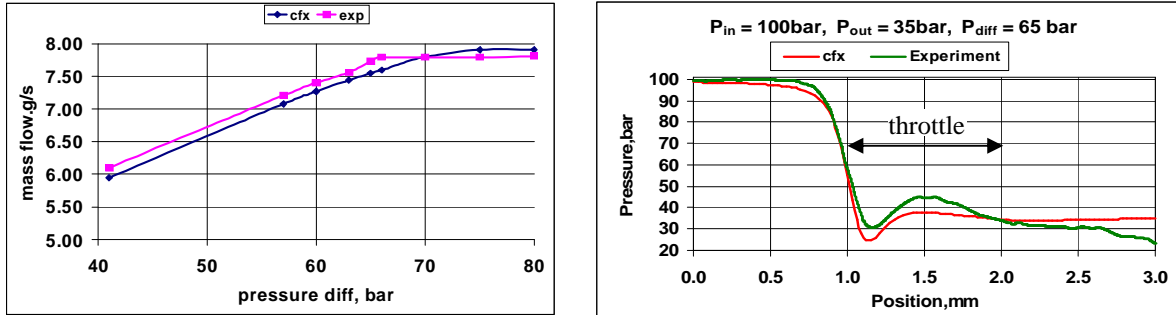


Figure 2. Comparison of numerical and experimental results. left) mass flow rate; right) centre line pressure.

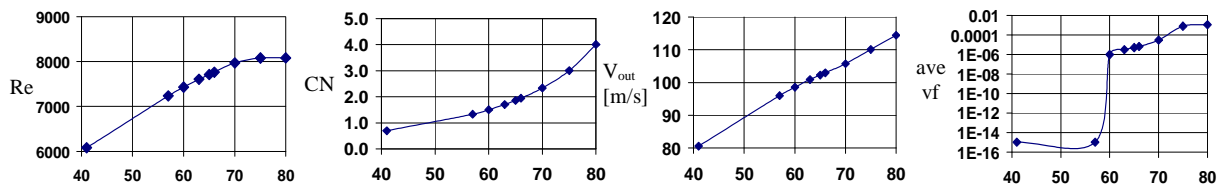


Figure 3. Reynolds number (Re), Cavitation number (CN), average throttle exit velocity, and average vapour volume fraction in computational domain corresponding to various pressure difference  $\Delta p$  in [bar]

It is interesting to have a look at the flow development along the throttle length. For that purpose, Figure 7 displays the centre plane velocity profiles at various distances away from the throttle entrance (nozzle J) for the case of  $\Delta p = 60$  bar and  $\Delta p = 80$  bar. Here  $d$  represents the throttle height. The x-axis is the dimensionless velocity normalized by the Bernoulli velocity, i.e.  $V^* = |V| / \sqrt{2\Delta p / \rho_l}$ , and the y-axis is the half throttle height in [ $\mu\text{m}$ ]. In the case  $\Delta p = 60$  bar, reverse flow close to the top wall together with strong flow acceleration and velocity overshoots ( $V^* > 1$ ) close to the separation zone were predicted in the throttle entrance region (till  $l/d = 0.85$ ). For  $l/d > 1$ , the flow becomes reattached to the top wall, the velocity profile becomes well developed, and the velocity overshoot phenomenon disappears. The distance needed for the flow development is similar in the case of  $\Delta p = 80$  bar. Nevertheless, velocity overshoots are observed in all profiles, extending from the near-wall region to the throttle centre with increasing  $l/d$  ratios. In this case, flow is choked in the throttle due to strong cavitation. The effective cross-section area of the flow path in the throttle is significantly reduced. This leads to the flow acceleration and the overall velocity overshoots at larger  $l/d$  ratios.

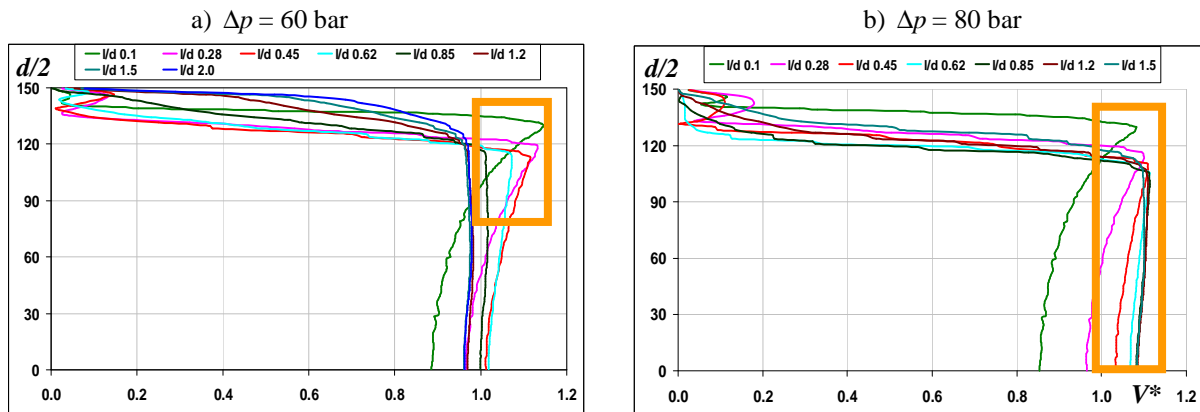


Figure 4. Development of center plane velocity profile [m/s] in throttle, the y-axis is throttle half height in [ $\mu\text{m}$ ]

Another phenomenon worth to mention is the vortex cavitation phenomenon in the throttle, which is demonstrated by Fig. 5 for the case of  $\Delta p = 75$  bar. Rotational vortices and vortex induced cavitation are typical features of hydraulic flow in fuel injection nozzles, see e.g. [7, 8]. These structures have significant impacts on liquid breakup and spray propagation behaviour.

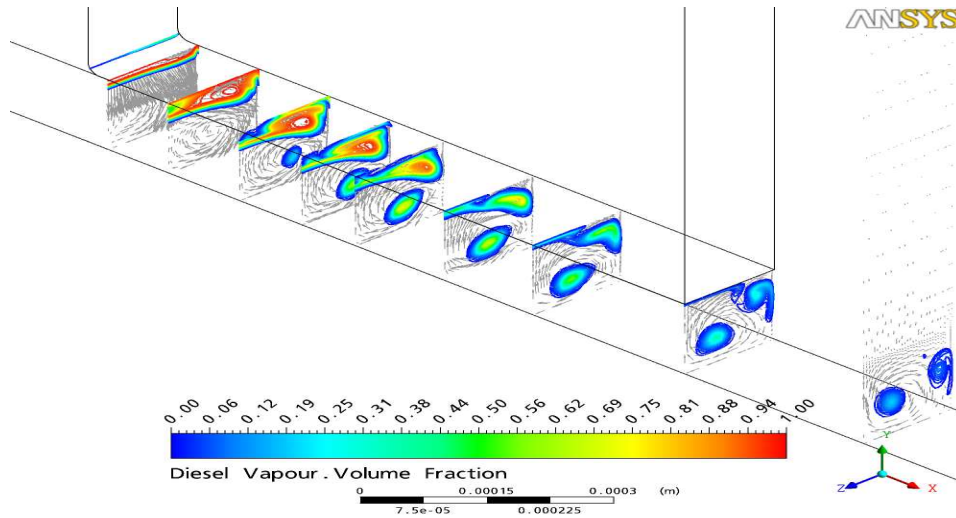


Figure 5. Vapor volume fraction distribution and velocity vectors over cross-section planes,  $\Delta p = 75$  bar

**Effect of saturation vapour pressure**

Gasoline fuels have much higher saturation vapour pressure than Diesel fuels, i.e. in the order of 0.8 bar vs. 0.035 bar under room temperature. With reference to the Rayleigh-Plesset equation for the bubble expansion, it is easily assumed that this difference is the major factor responsible for the much heavier cavitation in a gasoline fuel injection nozzle than in a Diesel nozzle under the same operating conditions. In order to evaluate the influence of the saturation vapour pressure on cavitation behaviour, we carried out simulations by using two different saturation vapour pressure values,  $p_b = 0.035$  bar and  $p_b = 0.8$  bar but keeping the rest fuel properties of the model Diesel unchanged. Surprisingly, the both sets of results show almost negligible differences in terms of vapour distribution in throttle, critical cavitation point, and mass flow rate (see Table 1). The reason for this might be due to the sharp pressure gradient in the throttle as can be observed from the pressure distribution (0 – 10 bar) plotted in Fig. 6 for the case of  $\Delta p = 80$  bar. The strong pressure gradient makes the pressure region between 0.035bar and 0.8bar negligibly narrow, which leads to the almost negligible effect of the saturation vapour pressure within this range of variation. In fact, the difference in viscosity between the gasoline and Diesel fuels is most responsible for the different cavitation behaviour of the two fuels, which is to be discussed below.

Table 1. Mass flow rate (g/s) under different saturation vapour pressure

| $\Delta p$ (bar) | Mass flow rate [g/s] |                   |
|------------------|----------------------|-------------------|
|                  | $p_b = 0.8$ bar      | $p_b = 0.035$ bar |
| 80               | 7.874                | 7.908             |
| 75               | 7.872                | 7.906             |
| 70               | 7.791                | 7.798             |
| 65               | 7.541                | 7.544             |
| 60               | 7.266                | 7.270             |

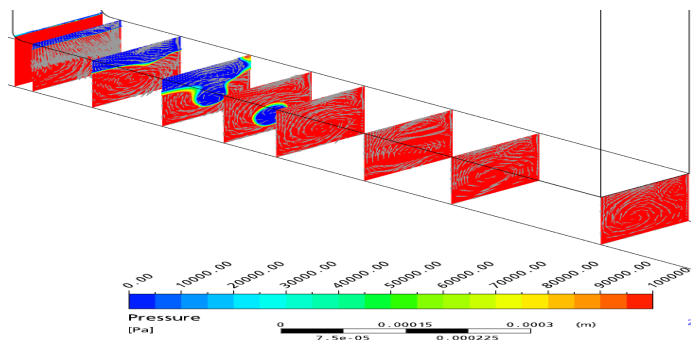


Figure 6. Pressure distribution in throttle J,  $\Delta p = 80$  bar

**Viscosity variation**

The investigation of the viscosity effect is based on the two viscosity values,  $\mu_l = 0.00325$  Pa s (the base case) and  $\mu_l = 0.001625$  Pa s, while keeping the other property values the same as the base case. The choice of the viscosity values is based on the consideration that the fuel viscosity can be halved with the fuel temperature

increasing from 25°C to 75°C, see e.g. [4]. The numerical results for mass flow rate ( $\dot{m}$ ), volume average of vapour volume fraction (ave vf) over the computational domain, ejection velocity at the throttle exit ( $V_{out}$ ), discharge coefficient ( $Cd = \frac{\dot{m}}{A_t \sqrt{2\rho_l \Delta p}}$ ), and Reynolds number (Re) are summarized in Table 2. For the convenience

of discussion, these results are also plotted in Fig. 7. It can be observed that reduction of viscosity increases the flow Reynolds number, causes stronger cavitation in the nozzle, and this further causes the flow to reach the critical cavitation point at lower  $\Delta p$  compared with the base case. Below the critical cavitation point, the flow of the lower-viscosity fuel has a 3% increase in mass flow rate or discharge coefficient than the base case. In comparison, these values are similar for both fuels in the choked flow regime. There is also a slight increase in the ejection velocity from the throttle exit (mass flow rate weighted average) in the lower viscosity flow due to the smaller viscous loss. These results confirm that Reynolds number is an important parameter for cavitating flow.

**Table 2.** Numerical results of viscosity variation

| a) $\mu_l = 0.00325 \text{ Pa}\cdot\text{s}$ |                    |                      |                    |       |      | b) $\mu_l = 0.001625 \text{ Pa}\cdot\text{s}$ |                    |                      |                    |       |       |
|--|--------------------|----------------------|--------------------|-------|------|---|--------------------|----------------------|--------------------|-------|-------|
| $\Delta p$<br>(bar)                          | $\dot{m}$<br>(g/s) | average<br>vapour vf | $V_{out}$<br>(m/s) | $Cd$  | Re   | $\Delta p$<br>(bar)                           | $\dot{m}$<br>(g/s) | average<br>vapour vf | $V_{out}$<br>(m/s) | $Cd$  | Re    |
| 80   | 7.91               | 1.165E-03            | 114.4              | 0.766 | 8083 | 80  | 7.94               | 1.471E-03            | 118.1              | 0.769 | 16232 |
| 75   | 7.91               | 8.25E-04             | 110.1              | 0.791 | 8082 | 75  | 7.94               | 1.151E-03            | 113.7              | 0.794 | 16230 |
| 70   | 7.80               | 3.11E-05             | 105.7              | 0.807 | 7971 | 70  | 7.94               | 7.36E-04             | 109.1              | 0.822 | 16225 |
| 65   | 7.54               | 5.23E-06             | 102.3              | 0.811 | 7712 | 65  | 7.73               | 1.18E-05             | 104.8              | 0.831 | 15802 |
| 60   | 7.27               | 9.94E-07             | 98.6               | 0.813 | 7431 | 60  | 7.46               | 2.95E-06             | 101.1              | 0.834 | 15251 |

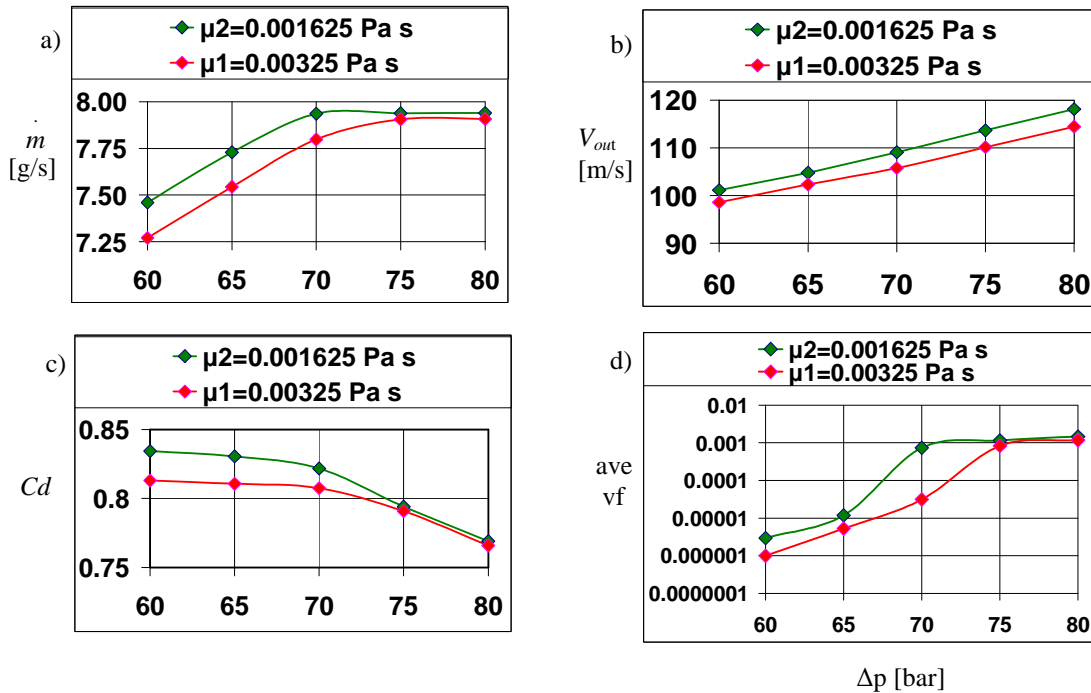


**Figure 7.** Numerical results of viscosity variation at various  $\Delta p$

In order to demonstrate the Reynolds number effect, the mass flow rate weighted average of a) absolute pressure  $P_{abs}$ , b) dynamic pressure  $P_{dyn} = \rho_l V_l^2 / 2$ , and c) the area average of the vapour volume fraction over the cross-section plane versus the throttle length ( $l/d$ ) are displayed in Fig. 8 for the cases of  $\Delta p = 60, 70,$  and  $80$  bar. The legend is shown for the inlet and outlet pressure, e.g. 100\_20 represents the case of 100 bar vs. 20 bar. As can be seen, lower viscosity (dash lines) leads to higher dynamic pressure and thus lower absolute pressure values and stronger cavitation in the throttle. This clearly indicates the Reynolds number effect, or the effect of the viscous vs. inertia ratio, on cavitation. The influence of viscosity can be much stronger in a real multi-hole fuel injection nozzle, where the flow is usually highly transient with hole-hole interaction.

In additional, it is worth noting that the flow experiences much stronger acceleration in the throttle entrance region and that the average dynamic pressure is much higher in the choked flow regime compared with the flow below the critical cavitation point. This is extremely obvious by comparing the corresponding two cases at  $\Delta p = 70$  bar.

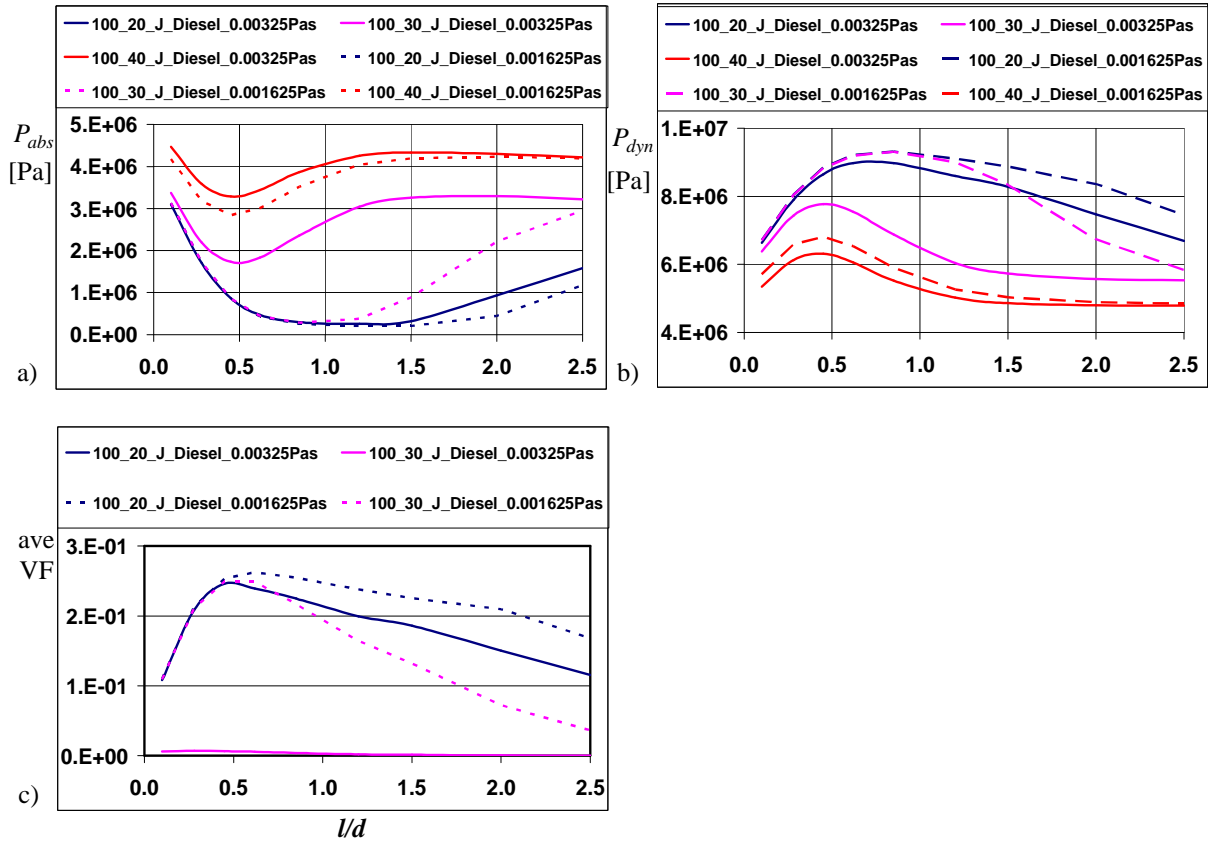


**Figure 8.** Distribution of cross-section average of a) absolute pressure, b) dynamic pressure, c) vapour volume fraction, along the along the throttle length ( $l/d$ )

**Density variation**

Simulations were carried out by using 4 different liquid fuel density values, namely  $828 \text{ kg/m}^3$ ,  $710 \text{ kg/m}^3$ ,  $533 \text{ kg/m}^3$ , and  $355 \text{ kg/m}^3$ , while keeping the rest of property values the same as the base case. The results for the mass flow rate, the volume average vapour volume fraction in the computational domain, the ejection velocity from the throttle exit, the discharge coefficient ( $Cd$ ), and the corresponding Reynolds number ( $Re$ ) are presented in Table 3 for the case  $\Delta p = 60$  bar. The kinematic viscosity decreases and the Reynolds number value (the inertia effect) increases with increasing density. This leads to stronger cavitation in the nozzle and a slight increase in the discharge coefficient. This is consistent with the results obtained from the viscosity variation study discussed above, but the effect of density variation on the discharge coefficient is much weaker than the viscosity variation. By the way, the reduction in ejection velocity for the higher density fuels can be understood with a reference to the Bernoulli equation.

It is interesting to note that cavitation is not incepted in the case of  $\rho_l = 355 \text{ kg/m}^3$  ( $Re = 4747$ ), even if the Cavitation number  $CN = 1.33$  is constant for all cases. This is a good proof of the inertia effect ( $Re$ ) on cavitation. Furthermore, the vapour volume fraction distributions plotted in Fig. 9 further confirm that cavitation increases with increasing inertia effect.

For the purpose of completeness, the results for the case of  $\rho_l = 710 \text{ kg/m}^3$  and  $\rho_l = 828 \text{ kg/m}^3$  under various  $\Delta p$  are summarized in Table 4. These results further support the above conclusions.

**Table 3.** Results of density variation at  $\Delta p = 60$  bar

| $\rho_l$<br>kg·m <sup>-3</sup> | $\dot{m}$<br>(g/s) | average<br>vapour vf | $V_{out}$<br>(m/s) | Re   | $Cd$  |
|--------------------------------|--------------------|----------------------|--------------------|------|-------|
| 828                            | 7.27               | 9.9E-07              | 98.6               | 7431 | 0.813 |
| 710                            | 6.69               | 6.8E-07              | 105.9              | 6847 | 0.809 |
| 533                            | 5.75               | 3.5E-07              | 121.0              | 5881 | 0.802 |
| 355                            | 4.64               | 0                    | 146.5              | 4747 | 0.793 |

**Table 4.** Results of density variation study at various  $\Delta p$

a)  $\rho_l = 828$  kg/m<sup>3</sup>

| $\Delta p$<br>bar | $\dot{m}$<br>(g/s) | average<br>vapour vf | $V_{out}$<br>(m/s) | $Cd$  | Re   |
|-------------------|--------------------|----------------------|--------------------|-------|------|
| 80                | 7.90               | 1.17E-03             | 114.4              | 0.766 | 8083 |
| 75                | 7.90               | 8.25E-04             | 110.1              | 0.791 | 8082 |
| 70                | 7.79               | 3.11E-05             | 105.7              | 0.807 | 7971 |
| 65                | 7.54               | 5.23E-06             | 102.3              | 0.811 | 7712 |
| 60                | 7.27               | 9.94E-07             | 98.6               | 0.809 | 7431 |

b)  $\rho_l = 710$  kg/m<sup>3</sup>

| $\Delta p$<br>bar | $\dot{m}$<br>(g/s) | average<br>vapour vf | $V_{out}$<br>(m/s) | $Cd$  | Re   |
|-------------------|--------------------|----------------------|--------------------|-------|------|
| 80                | 7.31               | 1.12E-03             | 122.9              | 0.765 | 7480 |
| 75                | 7.31               | 7.76E-04             | 118.2              | 0.790 | 7478 |
| 70                | 7.19               | 2.46E-05             | 113.8              | 0.805 | 7357 |
| 65                | 6.95               | 4.75E-06             | 110.0              | 0.807 | 7113 |
| 60                | 6.69               | 6.77E-07             | 105.9              | 0.809 | 6847 |

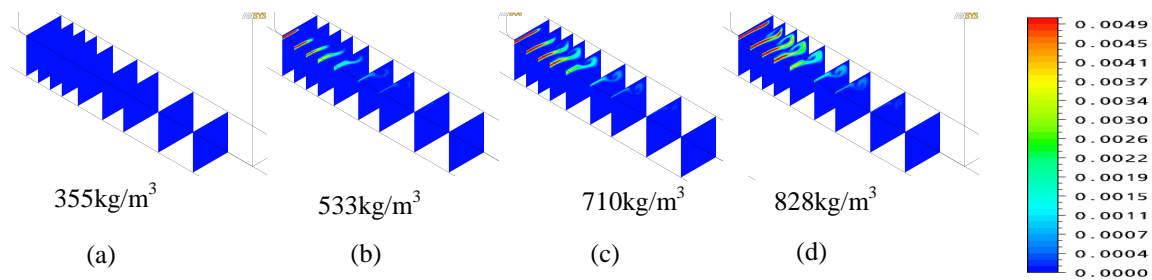


**Figure 9.** Vapor volume fraction distribution in throttle under variant density,  $\Delta p = 60$  bar

**Fuel variation & fuel temperature variation**

In order to evaluate the different cavitation behaviour of gasoline fuel and Diesel in the nozzle, simulations were also performed for the fuel n-heptane (denoted by NH), for the fuel temperature 20 °C and 70 °C, respectively, and for the nozzle geometry I (without inlet rounding) and geometry J (inlet rounding). The fuel n-heptane, whose properties are available from the ANSYS-CFX11.0 property database, was used to represent the gasoline fuel. An overview of the fuel properties under the above conditions is given in Table 5. It is worth noting that the kinematic viscosity of the model Diesel is about 5 times as high as the viscosity of n-heptane at 20 °C. In addition, there is an increase of about 40 percent in the n-heptane liquid viscosity and a reduction by 5 percent in density when the fuel temperature increases from 20 °C to 70 °C.

In practice application engineers often want to know how the mass flow rate changes with fuel temperature variation. The results presented in Table 6 indicate that the ratio of mass flow rate between the n-heptane fuel of 20 °C and 70 °C is more or less scalable with the square root of their density ratio ( $\approx 1.026$ ) based on the Bernoulli equation. Further results presented in Table 8 also support this conclusion except for the mass flow ratio between Diesel and n-heptane for  $\Delta p = 70$  bar and nozzle J. In this case, the mass flow rate ratio is about 1.10 compared with a value of 1.13 for the square root of the fuel density ratio. This exception is due to the fact that the flow of the n-heptane fuel at 70 °C has already reached choked flow regime, whereas the Diesel fuel flow in nozzle J is still below the critical cavitation point at  $\Delta p = 70$  bar (refer to the results in Table 1 and Table 6). The ratio of the ejection velocity from the nozzle I exit between Diesel and n-heptane fuel at 70 °C is also found to

be close to the density ratio  $\sqrt{\rho_{Diesel}/\rho_{NH}} = 1.13$ , whereas the corresponding velocity ratio for nozzle J is equal to 1.2, much higher than the square root of the density ratio.

**Table 5.** Overview of fuel properties

| Fuel     | T [°C] | Vapor pressure [bar] | Density [kg/m <sup>3</sup> ] | Viscosity [Pa·s] |
|----------|--------|----------------------|------------------------------|------------------|
| Diesel   | 20     | 0.035                | 828                          | 3.25e-3          |
| NH_20 °C | 20     | 0.05                 | 680                          | 4.697e-4         |
| NH_70 °C | 70     | 0.4                  | 646                          | 2.905e-4         |

**Table 6.** n-heptane temperature variation (geo J)

| $\Delta p$ | $\dot{m}$ (g/s) |        | mass ratio |
|------------|-----------------|--------|------------|
|            | T=20°C          | T=70°C |            |
| 80         | 7.22            | 7.03   | 1.03       |
| 70         | 7.21            | 7.03   | 1.03       |
| 67         | 7.20            | 7.02   | 1.03       |
| 65         | 7.13            | 6.98   | 1.02       |
| 60         | 6.89            | 6.73   | 1.02       |

**Table 7.** Results of fuel variation and fuel temperature variation for nozzle I and J

| $\Delta p$ (bar) | Nozzle | fuel    | mass flow rate (g/s) | $V_{out}$ (m/s) | Re    | $Cd$  |
|------------------|--------|---------|----------------------|-----------------|-------|-------|
| 80               | J      | Diesel  | 7.91                 | 114.4           | 8083  | 0.766 |
| 80               | J      | NH_70°C | 7.03                 | 137.1           | 80391 | 0.771 |
| 80               | J      | NH_20°C | 7.22                 | 133.0           | 51073 | 0.772 |
| 70               | J      | Diesel  | 7.8                  | 105.7           | 7971  | 0.872 |
| 70               | J      | NH_70°C | 7.03                 | 126.6           | 80383 | 0.89  |
| 80               | I      | Diesel  | 7.2                  | 108.7           | 7355  | 0.697 |
| 80               | I      | NH_70°C | 6.34                 | 120.4           | 72459 | 0.695 |
| 70               | I      | Diesel  | 7.19                 | 98.7            | 7349  | 0.804 |
| 70               | I      | NH_70°C | 6.32                 | 111.3           | 72413 | 0.802 |

**Table 8.** Mass flow rate & ejection velocity ratio: Diesel vs. NH 70 °C

| Nozzle | $\Delta p$ (bar) | Ratio Diesel vs. NH_70 °C                |  |                                    |                                    |  |
|--------|------------------|--|--|------------------------------------|------------------------------------|--|
|        |                  | $\sqrt{\frac{\rho_{Diesel}}{\rho_{NH}}}$ | $\sqrt{\frac{\mu_{Diesel}}{\mu_{NH}}}$ | $\sqrt{\frac{V_{Diesel}}{V_{NH}}}$ | $\sqrt{\frac{m_{Diesel}}{m_{NH}}}$ | $\sqrt{\frac{V_{out}^{NH}}{V_{out}^{Diesel}}}$ |
| J      | 80               |  |  |                                    | 1.13                               | 1.20   |
|        | 70               |  |  |                                    | 1.11                               | 1.20   |
|        |                  | 1.13                                     | 11.19                                  | 8.73                               |                                    |  |
| I      | 80               |  |  |                                    | 1.14                               | 1.11   |
|        | 70               |  |  |                                    | 1.14                               | 1.13   |

As is shown by Fig. 10, fuel temperature increase leads to enhanced cavitation in nozzle and stronger vortex cavitation. Nevertheless, this is mainly due to the reduction in fluid viscosity (by 40 percent) rather than the density change (about 5 percent) or the vapour pressure change, with reference to the results from single property variation discussed above. These results further confirm the Reynolds number effect on cavitation.

The results concerning the fuel property effect is consistent for both nozzle geometries. As is expected, nozzle J has higher flow efficiency for the inlet rounding, higher nozzle exit velocity (refer to Table 7 and [4]), reduced vapour production (refer to Fig. 11a, 11b), and postpones the critical cavitation point to higher injection pressure. Nevertheless, the vortex cavitation seems to be stronger for nozzle J in the choked flow regime (refer to Fig. 11c, 11d), indicating stronger vortex generation with inlet rounding.



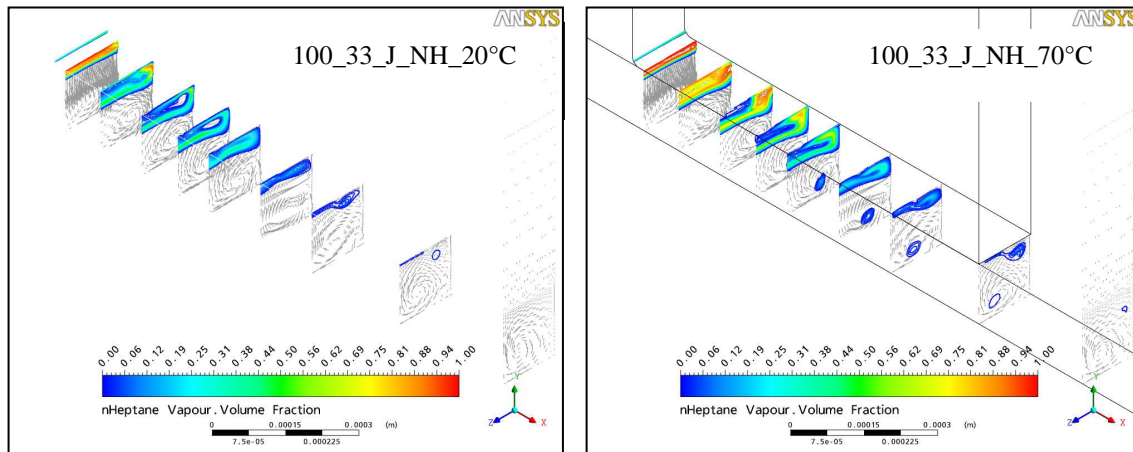


**Figure 10.** Vapour volume fraction distribution in nozzle J, comparison for n-heptane at 20 °C and 70 °C at 67 bar injection pressure

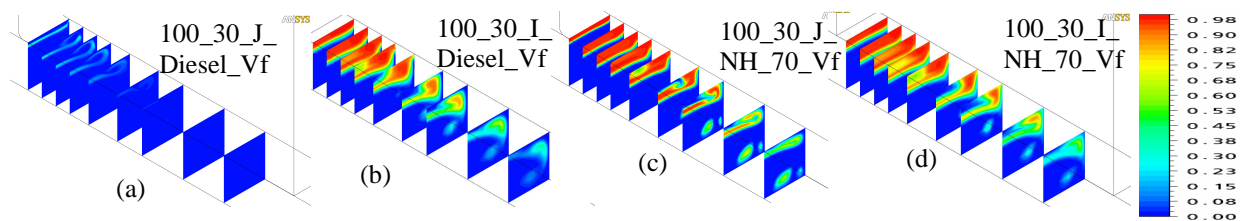


**Figure 11.** Comparison of vapour volume fraction distribution for Diesel and n-heptane 75 °C in nozzle I and J, at an injection pressure of  $\Delta p = 70$  bar

## Conclusion

The present study of fuel property effect on cavitation in generic nozzles of simple geometries has led to the following conclusions:

Fuel saturation vapor pressure variation up to 0.8 bar has no essential effect on cavitation. This is due to the very high pressure gradient caused by the flow acceleration in the nozzle.

Both fluid viscosity and density change have a significant effect on cavitation. Keeping the other properties constant, decreasing viscosity or increasing density leads to increasing flow Reynolds number and inertia effect, stronger flow acceleration and enhanced cavitation in a nozzle, and to a slight increase in flow efficiency in the flow regime below the critical cavitation point.

Viscosity varies much stronger than density from fuel to fuel or when fuel temperature changes, and thus has the most significant effect on cavitation.

Within the same flow regime, the variation of mass flow rate in response to fuel temperature change or fuel change is more or less scalable by the square root of the fuel density ratio. The nozzle exit velocity increases with reducing fluid density, but is found to be not scalable by the density ratio. In comparison, reduction in viscosity will cause a minor increase in mass flow rate and in nozzle exit velocity.

## References

- [1] Perković L, Greif .D, Tatschl R., Priesching P., Duić N., *3D CFD Calculation of Injector Nozzle Model Flow for Standard and Alternative Fuels*, HEAT 2008, Fifth International Conference on Transport Phenomena In Multiphase Systems June 30 - July 3, 2008, Bialystok, Poland.
- [2] Lee H-K, Russell M.F., Bae C.S. and Shin H. D., *Development of cavitation and enhanced injector models for diesel fuel injection system simulation*, Proceedings of VAFSEP2004, 6-9 July 2004, Dublin, Ireland.
- [3] Suh H. K, Park S. H., Lee C. S., *Experimental Investigation of Nozzle Cavitating Flow Characteristics for Diesel and Biodiesel Fuels*. International Journal of Automotive Technology, Vol. 9, No. 2, pp. 217-224, 2008.
- [4] Zigan.L , Schmitz I., Wensig M., Leipertz A., *Effect of Fuel properties on primary breakup and spray formation studied on a gasoline 3-hole nozzle*, ILASS-Europe 2010, 23rd Annual Conference on Liquid Atomization and Spray Systems, Brno, 2010.
- [5] Menter F, *Zonal two equation k- $\omega$  turbulence models for aerodynamic flows*. AIAA Journal, 93-2906, 1993.

- [6] Zwart P.J, Gerber A., and Belamri T. *A two-phase flow model for predicting cavitation dynamics*. Int Conf on Multiphase Flow, Paper No 152, 2004.
- [7] Shi J.-M., Wenzlowski K., Helie J., Nuglisch H. and Cousin J., *URANS & SAS analysis of Flow Dynamics in a GDI nozzle*. ILASS-Europe 2010, 23rd Annual Conference on Liquid Atomization and Spray Systems, 2010, Brno, 2010.
- [8] Shi J.-M., Helie J., Khan M., Cousin J., *The role of unsteadiness and coherent structure in the internal flow of automotive injectors: LES improving the understanding of the atomisation generation*, submitted to LES for Internal Combustion Engine Flows, 18 - 19 November 2010, Rueil-Malmaison, France.

## Nomenclature

|            |   |
|------------|---|
| $A_t$      | Throttle cross-section area [m <sup>2</sup> ]                                   |
| $C_d$      | Discharge co-efficient  |
| $CN$       | Cavitation number   |
| $d$        | Throttle height [m]   |
| $F_1$      | Vaporization coefficient  |
| $F_2$      | Condensation coefficient  |
| $L_t$      | Characteristic length [m]   |
| $l/d$      | Length to height ratio  |
| $\dot{m}$  | Mass flow rate [g/s]  |
| $p$        | Pressure [bar]  |
| $P_{in}$   | Inlet pressure [bar]  |
| $P_{out}$  | Back pressure [bar]   |
| $\Delta p$ | Pressure difference / Injection pressure [bar]                                  |
| $p_b$      | Vapor saturation pressure [bar]   |
| $R_b$      | Nuclei bubble radius [m]  |
| $S_{lv}$   | Cavitation induced mass source/sink term [kg·m <sup>-3</sup> ·s <sup>-1</sup> ] |
| $T$        | Temperature [°C]  |
| $U_i$      | Velocity in the direction x [m·s <sup>-1</sup> ]                                |
| $U_j$      | Velocity in the direction y [m·s <sup>-1</sup> ]                                |
| $V_{out}$  | Throttle outlet velocity [m·s <sup>-1</sup> ]                                   |
| $\nu_f$    | Vapour volume fraction  |
| $V^*$      | non-dimensional velocity  |
| $\alpha$   | Vapor volume fraction   |
| $\alpha_0$ | Initial cavitation nuclei volume fraction                                       |
| $\mu$      | Dynamic viscosity [Pa·s]  |
| $\mu_m$    | Mixture dynamic viscosity [Pa·s]  |
| $\mu_{mt}$ | Mixture eddy viscosity [Pa·s]   |
| $\mu$      | Dynamic viscosity [Pa·s]  |
| $\rho$     | Density [kg·m <sup>-3</sup> ]   |
| $V$        | Velocity [m·s <sup>-1</sup> ]   |

## Subscripts

|      |                   |
|------|-------------------|
| $t$  | throttle          |
| $B$  | bubble            |
| NH   | n-heptane         |
| $m$  | mixture           |
| $mt$ | mixture turbulent |
| $l$  | liquid            |
| $v$  | vapor             |